Macromolecules

ARTICLE

pubs.acs.org/Macromolecules

Equilibrium Structure and Dynamics of Self-Associating Single Polymers

Charles E. Sing and Alfredo Alexander-Katz*

Department of Materials Science and Engineering, Massachusetts Institute of Technology, Cambridge, Massachusetts 02139, United States

Supporting Information

ABSTRACT: There has been significant interest recently in the development of materials that utilize the kinetic properties of self-associating groups, which can be tuned to manipulate dynamics and control mechanical, optical, and rheological properties. Here we describe the single-chain behavior of self-associating polymers in solution, using results from both simulation and theory. We use Brownian dynamics simulations with monomers that can reversibly associate using Bell model-based reaction kinetics. A straightforward two-state model is considered, and associations are exclusive; however, generalizations beyond these behaviors are briefly considered in the theory. We demonstrate that, even for a Θ-polymer, the inclusion of self-associations can drive the polymer into an equilibrium structure that resembles a collapsed polymer globule. The dynamic behavior of these polymers exhibits two regimes, with Rouse-dominated time scales when binding reactions have low energetic barriers and binder-dominated time scales when binding reactions have large energetic barriers. These results have implications in a diverse array of applications ranging from supramolecular chemistry to stimuli responsive materials to biological polymer dynamics.

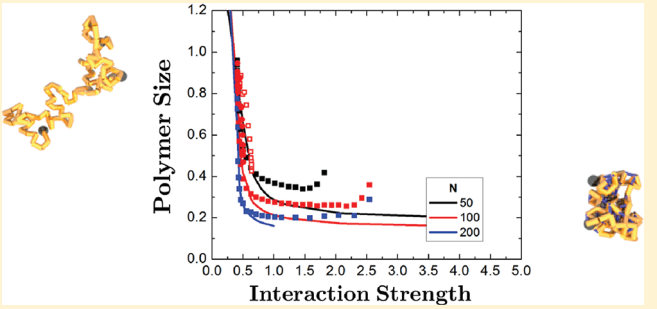

INTRODUCTION

Polymeric materials are often advantageous to use due to the relative ease in which disparate time scales can be accessed. Parameters such as molecular weight, chemical structure, and temperature govern the dynamic properties of most polymer systems in ways that are well characterized.[1,2] Recently, however, the use of reversible supramolecular associations has been demonstrated to be a powerful route to tune material properties in useful and novel ways.[3−10] These materials use reversible chemistry, such as hydrogen bonds, metal−ligand coordination, or reversible covalent bonding, to adjust the response of the material to various stimuli (mechanical, electromagnetic, thermal, etc.).[6] Many of these applications have in turn been described through a number of simulation and theoretical models, most notably the work by Liebler, Rubinstein, and Colby.[9,11−23] The crucial feature of all of these models is the inclusion of a new, reaction-dependent time scale that governs the network rearrangement of the material.[11−13,21−23]

The inspiration for many of these materials comes directly from biological systems, where such reversible associations are known to drive a large number of processes from the molecular to physiological levels.[4,8,24−28] On the large scale tissue-level, a large amount of research has focused on mimicking modulus change or mechanical actuation that is seen in biology through the use of the properties of associating networks and gels.[3,4,6,8,29,30] Effects such as percolation and swelling are driving mechanisms for mechanical response that, through the introduction of reversible associations, have characteristic time scales that can be manipulated.[5,29] Parallel strains of research seek to understand single-molecule behaviors of biopolymers through the use of tools such as atomic force microscopy and optical tweezing to supplement simulation and theory on protein conformational behavior, and recent research has aimed to introduce supramolecular chemistry principles as a way to create single molecules with novel response characteristics.[4,8,28,31−35]

The equilibrium and dynamics of single molecules is a widely studied field, and polymers with strong self-interactions comprise of a large subset of this field that is concerned with the collapsed globule state of polymers.[1,2,25,26,31,36−38] This state of polymer is hard to access experimentally; however, collapsed polymers are widely considered to be a relevant starting point for the understanding of protein and other biopolymer behaviors.[31,33−35,39,40] A wide array of studies exist in the literature, including investigations into the equilibrium state of a globule,[41−43] its pulling profile under a constant load,[33,44] and its structural characteristics as it undergoes collapse from an extended or coiled state.[39,40,45−49] The dynamics of the latter transition have been well documented, with the strength of the polymer self-interactions and hydrodynamic interactions being particularly important considerations, along with chain sequence if a heteropolymer is considered.[39,40,45−49] Despite this wealth of literature, most current theoretical and simulation

Received: April 10, 2011
Revised: July 1, 2011
Published: August 17, 2011

developments have considered effective interaction potentials such as Lennard-Jones potentials that serve to coarse grain more specific types of interaction.[33,39−41,45,47,48,50] This type of model has proven to be very successful in describing interactions that occur on subchain time scales, such as dispersive and hydrophobic forces; however, it neglects the dynamic features present in other common interaction types, such as hydrogen bonds or reversible covalent bonding.[37,38] More specifically, there is no ability to adjust the interaction kinetics, which we will show is essential in determining the overall conformational dynamics of a single polymer chain. This becomes incredibly important in the context of properties that are coupled to external forces that can drive chain and interaction kinetics, such as forces due to fluid flows or other types of mechanical loads.

To investigate the effect of interaction kinetics on the dynamics of single-chain polymers, we use a Brownian dynamics (BD) simulation with "reaction" interactions that allow for the adjustment of both equilibrium and dynamic behaviors through a simple two-state reaction model in a fashion similar to Hoy and Fredrickson.[20] We can show that, by favoring the presence of the bound reaction state, we can cause the polymer to collapse in a way that is analogous to the collapse of a polymer model that utilizes Lennard-Jones behavior. We develop a straightforward theory to provide a direct comparison between both models that can account for both periodicity and exclusivity effects. While the equilibrium structure can be directly compared to the collapsed globule state of a polymer, the conformational dynamics of this polymer can be strongly altered by the influence of the reaction kinetics. We identify two regimes; with quick reaction kinetics the Rouse time scale dominates the conformational dynamics, while with slow reaction kinetics the binder time scales dominate. This, in principle, enables one to slow down the polymer relaxation time scales without affecting the equilibrium structure. We provide a simple theory to describe this behavior using straightforward modifications of the Rouse theory of polymer dynamics.

SIMULATION METHODS

We consider a polymer consisting of N beads of radius a in a potential U. We use a Brownian dynamics (BD) simulation, which is performed by numerically integrating the Langevin equation for a given bead i at position $\mathbf{r}_i$:

$$\frac{\partial}{\partial t}\mathbf{r}_i = -\sum_j \boldsymbol{\mu}_{ij}\cdot\nabla_{\mathbf{r}_j}U(t) + \boldsymbol{\xi}_i(t) \tag{1}$$

where $\boldsymbol{\mu}_{ij}$ is the mobility matrix, $\boldsymbol{\xi}_i$ is a random velocity that satisfies $\langle\boldsymbol{\xi}_i(t)\boldsymbol{\xi}_j(t')\rangle = 2k_BT\boldsymbol{\mu}_{ij}\delta(t-t')$. In this investigation, we consider only simulations of freely draining (FD) polymers, so the mobility matrix has the form $\boldsymbol{\mu}_{ij} = (1/6\pi\eta_s a)\delta_{ij}\mathbf{I}$ where $\boldsymbol{\eta}_s$ is the solvent viscosity and $\mathbf{I}$ is the identity tensor.[36] The FD case assumes the absence of hydrodynamic interactions, such that a given bead feels a drag that is proportional only to its velocity.[36] The addition of hydrodynamic interactions was not done for purposes of computational expediency, since the inclusion of this effect would simply replace the Rouse relaxation time τ_R with the Zimm relaxation time τ_Z in the theory.

The potential energy $U = U_S + U_{LJ} + U_{RXN}$ is a sum of three contributions, representing connectivity, excluded volume, and reaction potentials, respectively. The connectivity potential U_S is a harmonic spring potential that acts between adjacent beads along the chain:

$$U_S = \frac{\kappa}{2}k_BT\sum_{i=1}^{N-1}(r_{i+1,i}-2a)^2 \tag{2}$$

where $r_{i,j}$ is the distance between beads i and j and $\kappa = 500/a^2$ is a spring constant that is strong enough to limit chain stretching to a negligible level. The Lennard-Jones potential U_{LJ} is the interaction potential between any pair of adjacent beads:

$$U_{LJ} = \tilde{u}_{LJ}k_BT\sum_{ij}\left[\left(\frac{2a}{r_{ij}}\right)^{12} - 2\left(\frac{2a}{r_{ij}}\right)^{6}\right] \tag{3}$$

where $\tilde{u}$ determines the depth of the potential in units of k_BT. This is the potential typically used to cause collapse of polymers in Brownian dynamics models, and the relationship between $\tilde{u}_{LJ}$ and chain dimensions is well understood and corresponds well to experimental results of chain collapse via hydrophobic forces. For our simulations, we use a constant value $\tilde{u}_{LJ} = 0.41$, which corresponds to the Θ temperature where there is no net monomer−monomer interaction.[33,36] Our model also accounts for chemical reaction-based reversible associations, using the potential U_{RXN} that is only present if two adjacent monomers have reacted:

$$U_{RXN} = \frac{\kappa}{2}k_BT\sum_{i,j}^{N}\Omega(i,j)(r_{i,j}-2a)^2 \tag{4}$$

where $j \neq (i, i-1, i+1)$. $\Omega(i,j)$ is a function such that $\Omega(i,j) = 1$ if there is an association between i and j, but $\Omega(i,j) = 0$ otherwise. The calculation of $\Omega(i,j)$ occurs once in every time interval τ_0, at which point there is a Monte Carlo type update step governed by the following:

$$\Omega(i,j,t) = \begin{cases} \begin{cases} 1 & \Xi < e^{-\Delta E_B} \\ 0 & \Xi > e^{-\Delta E_B} \end{cases} & \text{if } \Omega(i,j,t-\tau_0) = 0 \cap r_{ij} < r_{rxn} \\ \begin{cases} 0 & \Xi < e^{-\Delta E_{UB}} \\ 1 & \Xi > e^{-\Delta E_{UB}} \end{cases} & \text{if } \Omega(i,j,t-\tau_0) = 1 \end{cases} \tag{5}$$

where the state of a given component of $\Omega(i,j,t)$ depends on the binding transition probability (given by $e^{\{-\Delta E_B\}}$ and $e^{\{-\Delta E_{UB}\}}$), the previous state ($\Omega(i,j,t-\tau_0)$), and the juxtaposition of the beads i and j. Ξ is a random number between 0 and 1, and r_{rxn} is a reaction radius within which the reaction may occur. ΔE_B and ΔE_{UB} are energies (in k_BT) describing the reaction energy landscape. ΔE_B and ΔE_{UB} represent the activation energies of binding and unbinding, respectively, and are always positive. The overall energy difference between the bound and unbound states is thus $\Delta E_0 = \Delta E_B - \Delta E_{UB}$, where a decrease in ΔE_0 signifies more binding.

To simulate this model of a reacting polymer, eq 1 is discretized with a time step $\Delta t = 5 \times 10^{-4}\tau$, where $\tau = 6\pi\eta_s a^3/(k_BT)$ is the characteristic monomer diffusion time (the time that it takes a single simulation bead to diffuse its own radius a). Values are rendered dimensionless with lengths scaled by a, times scaled by τ, and energies scaled by k_BT and are indicated with tildes in the remainder of this article. The reaction values are chosen to be $\tau_0 = 0.1\tau$ and $\tilde{r}_{rxn} = 2.1$, such that $\tau_0^{1/2} > (\tilde{r}_{rxn} - 2)$, which ensures that in principle an unbinding bead can readily diffuse away from its bound partner. We apply an exclusivity constraint such that a given monomer can only bind

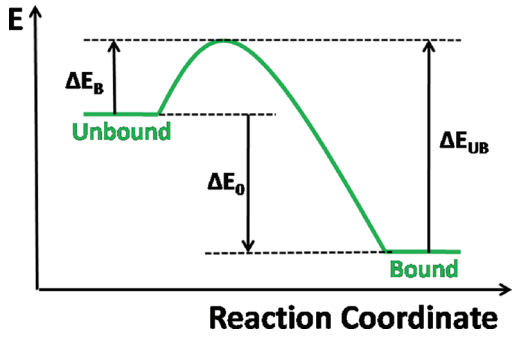

Figure 1. The energy landscape of a binding−unbinding transition for two adjacent beads. We consider only two states: an unbound state where two beads only interact through the standard Lennard-Jones potential for a Θ-polymer and a bound state where there is a harmonic spring connecting the two binding beads. There is an overall change in energy upon binding ΔE_0, which results from the difference in activation barriers for forward (ΔE_B) and backward (ΔE_{UB}) reactions.

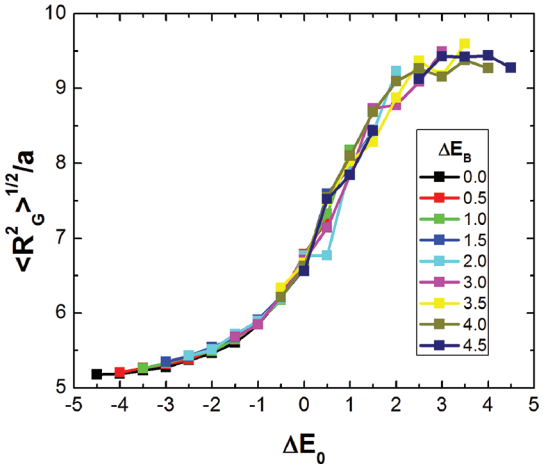

Figure 2. A plot of size $\langle R_G{}^2\rangle^{1/2}$ as a function of binding energy ΔE_0 for a number of activation energies, designated by ΔE_B (see Figure 1). All values of ΔE_B fall along the same universal curve, demonstrating that the equilibrium structure for globules collapsed by reaction mechanisms is only determined by ΔE_0.

to one other monomer at any given time:

$$\sum_j \Omega(i,j,t) \leq 1 \tag{6}$$

This can be relaxed if multifunctional association is desired, and binding order is randomized to ensure that binding is not biased toward beads of lower index.

RESULTS AND DISCUSSION

In understanding the behavior of self-associating polymers, we seek to examine both the equilibrium properties and dynamic properties of chains in our simulations and then draw the appropriate comparisons to chains that have similar structure using only Lennard-Jones interactions (Lennard-Jones polymers). Presumably, self-associating polymers can be manipulated by both types of behaviors simultaneously, with Lennard-Jones interactions representing hydrophobic and dispersive interactions

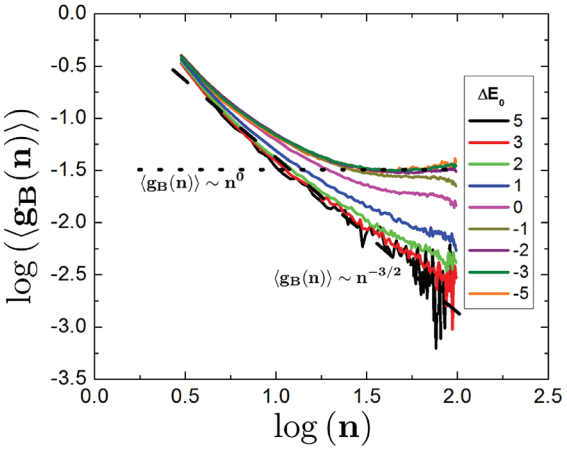

Figure 3. A log−log plot of the correlation function $\langle g_B(n)\rangle$ as a function of the distance between two beads n. For a Θ-polymer, there should be a scaling of $\langle g_B(n)\rangle \sim n^{-3/2}$ which is characteristic of a Gaussian chain. A number of curves representing different of values of ΔE_0 are plotted, along with a dashed line representing this $n^{-3/2}$ scaling. Clearly, as ΔE_0 is decreased, large deviations from this behavior occur. At very low values of ΔE_0, there are two regimes. At low values of n, the typical Θ-polymer behavior remains; however, at higher values of n the scaling becomes $\langle g_B(n)\rangle \sim n^0$. This is shown on the graph by the dotted line. This behavior is characteristic of polymer globule structure.

and the reaction associations representing hydrogen or reversible covalent bonding. Here we consider only two "pure" cases: (i) one where $\Omega(i,j,t) = 0$ for all i, j, and t, which represents a simple Lennard-Jones polymer where we adjust $\tilde{u}_{LJ}$, and (ii) one where $\tilde{u}_{LJ}$ is fixed at $\tilde{u}_{LJ} = 0.41$ (corresponding to a Θ-polymer) and varying $\Omega(i,j,t)$. As mentioned above, we consider only these two extremes; however, real systems may incorporate both behaviors simultaneously.

Equilibrium Structure. We measure the structure of these polymers through the characterization of conformational, binding, and chain correlation statistics. We run simulations for $>5 \times 10^8$ time steps to obtain good averages and discard the initial 1×10^6 time steps to allow for conformational equilibration. Statistics based on long, single runs are sufficient for the data presented, since generally the length of the run is much larger than the relaxation time of the system. $N = 100$ is used in this study (unless mentioned otherwise). We can calculate the size of the polymer as a function of the characteristics of the energy landscape described by any two of the three parameters ΔE_B, ΔE_{UB}, and ΔE_0 (see Figure 1 for a schematic). In Figure 2 we plot for a number of energy barriers ΔE_B the mean-squared radius of gyration $\langle R_G{}^2\rangle \approx (1/N)\Sigma_i^N\langle(\mathbf{r}_i - \mathbf{r}_{com})^2\rangle$ vs ΔE_0, where $\mathbf{r}_{com}$ is the polymer center of mass. As expected, all results follow a single universal $\langle R_G{}^2\rangle$ vs ΔE_0 curve regardless of the activation energy of going from one state to another, which indicates that only the relative energy difference between the bound and unbound states dictates the equilibrium structure while the energy barriers do not.

The equilibrium $\langle R_G{}^2\rangle$ vs ΔE_0 curve demonstrates that, by decreasing the relative energy of the bound state (thus increasing its prevalence), we can shrink the chain dimensions to well below those of a random-walk coil. Indeed, we see that self-associations can drive this polymer into a globule conformation. This is more clearly seen by considering a binding correlation function $\langle g_B(n)\rangle$ that describes the normalized probability of binding two

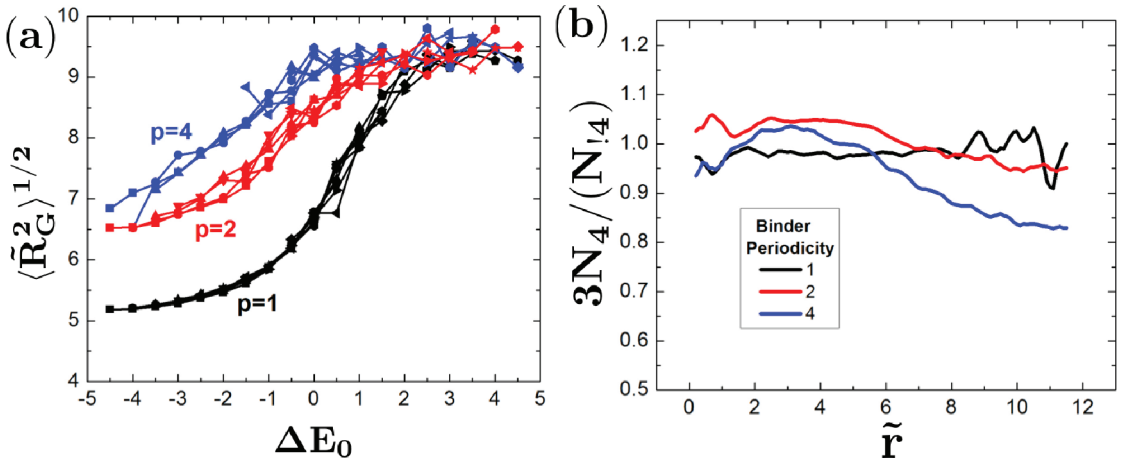

Figure 4. (a) The root-mean-square radius of gyration $\langle R_G^2 \rangle^{1/2}/a$ as a function of the reaction energy ΔE_0 for a number of periodicities p. As p increases, the extent of collapse strongly decreases. $N = 100$ for all values of p, and data are aggregated from simulations with low ΔE_B and ΔE_{UB} such that the equilibrium state is observed. (b) Comparison of the relative probabilities of finding a binder that has an index of multiple of 4 (N_4) vs a binder that is not a multiple of 4 ($N_{!4}$). This metric $3N_4/N_{!4}$ describes the relative amount of binders radially from the center of mass ($\tilde{r}$) for $p \neq 1$. Thus, the case $p = 1$ is roughly flat and centered on $3N_4/N_{!4} = 1$, while $p = 2$ and $p = 4$ demonstrate an abundance of binding beads in the center. As the length of nonbinding chain separating two binders increases, there is an increased tendency for the binders to partition to the center of the globule. $N = 100$ and $\Delta E_0 = -4$.

monomers that are located n beads apart along the polymer chain:

$$\langle g_B(n) \rangle = \frac{1}{N-n} \left\langle \sum_{i}^{N-n} \Omega(i, i+n) \right\rangle \quad (7)$$

where the angled brackets represent a time average. We plot this in Figure 3 for a variety of values of ΔE_0. This correlation function should scale as $\langle g_B(n) \rangle \sim n^{-3/2}$ for a Gaussian coil, and we retain this result in the limit of large positive values of ΔE_0 ($\Delta E_B > \Delta E_{UB}$). As ΔE_0 decreases, the large n behavior crosses over to $\langle g_B(n) \rangle \sim n^0$, but the small n behavior retains the Gaussian scaling.[51] This indicates that the polymer transforms to a globule-like structure, where the chain remains Gaussian only up to the point where the edge of the globule is encountered and points at larger contour distances become spatially uncorrelated. Thus, this transition is structurally an association-induced coil−globule transition.

The above data are given for a straightforward model that considers each bead to contain a single binder. This simulation model can be easily modified to consider chains that have less binders, and we define a periodicity parameter p that indicates that a binder occurs every p monomers. The majority of this data represents the condition $p = 1$; however, we also run simulations where $p = 2$ and $p = 4$. Unsurprisingly, the lower density results in a smaller extent of chain collapse as shown in Figure 4a. As p increases, however, we notice a decrease in globule/coil homogeneity, as we approach the flower micelle morphology predicted by Semenov et al. for chains with only a few associating groups connected by long linker chains.[12,13] This morphology is characterized by the accumulation of binders at the center of the globule so interactions are maximized, while nonbinding monomers are pushed to the outside of the globule. With $p = 4$ and $p = 2$, this effect is relatively weak; however, there is indeed a marked accumulation of the binders at the center of the globule on average, as shown in the radial binder distribution function shown in Figure 4b. In this graph, we calculate the average number of beads at a location $\tilde{r}$ from the center of mass of the globule that have an index that is a multiple of 4 (N_4) and that do not have an index that is a multiple of 4 ($N_{!4}$). Since the latter should be 3 times more prevalent in a completely homogeneous globule, the parameter $3N_4/N_{!4}$ should equal 1 in this case. This is indeed true for $p = 1$. For $p > 1$, however, we see an accumulation of binders at low $\tilde{r}$ ($3N_4/N_{!4} > 1$) and a depletion

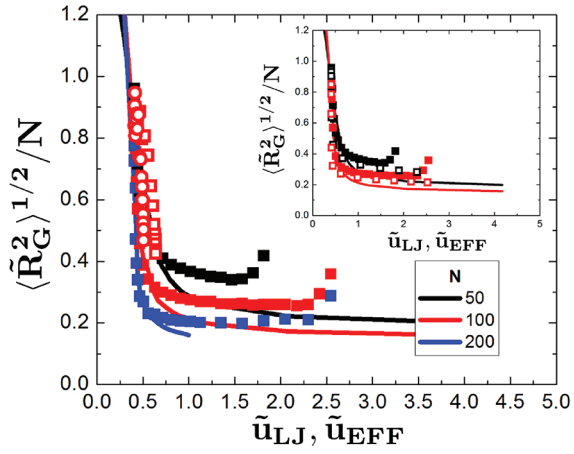

Figure 5. Collapsing behavior of a Lennard-Jones polymer (solid lines) described by plotting $\langle R_G^2 \rangle/N$ as a function of the Lennard-Jones interaction parameter $\tilde{u}_{LJ}$. Equation 9 is used to replot data like that seen in Figure 2 as a function of an "effective" interaction parameter $\tilde{u}_{EFF}$ that corresponds to $\tilde{u}_{LJ}$. Data are shown for $p = 1$ (filled squares), $p = 2$ (open squares), and $p = 4$ (open circles). There is a different extent of collapse seen in reacting polymers due to the presence of topological effects that prevents the realization of full chain collapse. This effect can be lowered by including difunctional binding, rather than making binding exclusive. The inset shows the effect of difunctional binding by plotting $N = 50$ (black) and $N = 100$ (red) for both monofunctional (filled symbols) and difunctional (open symbols) binding. Difunctional points are plotted using the effective energy term described in eq 11. Polymers with difunctional binders are driven to a more collapsed state; however, full Lennard-Jones comparison is still not completely possible. All points on these figures have error bars smaller than the size of the symbols.

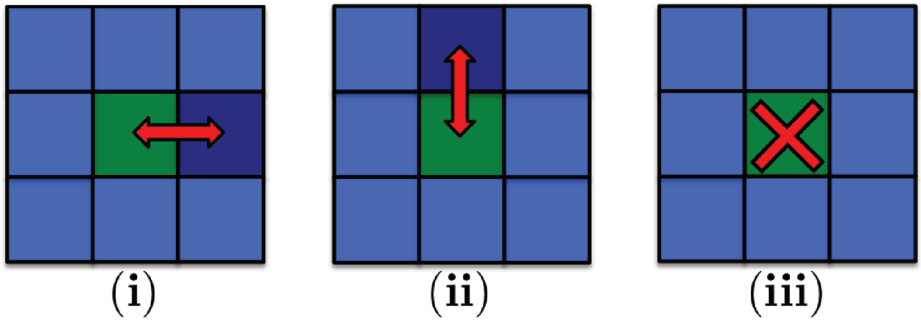

Figure 6. Lattice picture of the interior of a collapsed globule with self-associating behavior. A given binder (green lattice site) can bind to any of z neighbors (blue lattice sites) through a binding association (red arrow). This behavior is shown in (i) and (ii), which each demonstrate a binding possibility. There is also a probability $p_{UB} = (1 + e^{-\Delta E_0})^{-z}$ that a given binder is not bound to any of its neighbors, which is shown in (iii). By enumerating the probability of being bound versus unbound in this type of system, it is possible to describe the corresponding "effective" interaction parameter $\tilde{u}_{eff}$ that would give the same behavior in a Lennard-Jones system.

of binders at high $\tilde{r}$ ($3N_4/N_{!4} < 1$). We expect that longer nonbinding chains would strongly amplify this trend. This behavior is potentially useful; the accumulation of binders at the center of the polymer may enable the experimental realization of collapsed polymers that are resistant to large-scale aggregation due to the "hiding" of binders in the center of the globule.

The relationship shown in Figure 2 between the binding energy ΔE_0 and the size $\langle R_G^2 \rangle$ is quite different from what is seen for models using Lennard-Jones interactions that compare the $\langle R_G^2 \rangle$ to the parameter $\tilde{u}_{LJ}$.[36,41,45,47] The collapse transition is shown in Figure 5 for a number of polymers ($N = 50, 100, 200$) as $\tilde{u}_{LJ}$ is increased (solid lines).[36] The Lennard-Jones model is well-studied, so we will not dwell on its properties as it collapses.[52] It is possible, however, to understand the relationship between equilibrium structures of the two different systems. This difference can be described via a straightforward accounting of the states in which adjacent monomers can reside, which is performed over long time-averages to obtain sufficient sampling with slow binding kinetics. We use a lattice model to determine a mean-field equation that will describe the correspondence of a binding energy ΔE_0 and an "effective" Lennard-Jones parameter $\tilde{u}_{EFF}$ that time-averages the binding interactions such that they appear equivalent to Lennard-Jones interaction.

Our model (schematically shown in Figure 6) considers a binding bead that is directly adjacent to z neighboring beads that are within radius $\tilde{r}_{rxn}$ and thus can bind to any of them. It is either in a bound or an unbound state, with a probability p_B of being in the bound state. For a given pair of beads, such that $z = 1$, there is a probability that the beads are not bound $p_{UB}(z = 1) = 1/(1 + e^{-\Delta E_0})$. We can then calculate the probability that one of those beads does not bind to any of z neighboring beads p_{UB}:

$$1 - p_B = p_{UB} = (1 + e^{-\Delta E_0})^{-z} \quad (8)$$

which is equal to the fraction of binders that are unbound ($f_{UB} = p_{UB}$). Likewise, we consider an effective $\tilde{u}_{EFF}$ that time-averages the reacting polymer interactions such that they behave like a Lennard-Jones interaction. To build this equation, we use the approximation that a Lennard-Jones interacting bead with z neighbors has discretized states such that it is either interacting with all its neighbors with an energy $-z\tilde{u}_{LJ}$ or not interacting such that energy is 0. The probability that it is interacting at a given time is thus $(1 + e^{-z\tilde{u}_{LJ}})^{-1}$. For an associating polymer, our simulations include Lennard-Jones interactions (which we indicate as $\tilde{u}_0$), so an equation of this form will also be relevant when there is not already a binding association. We then equate the interacting probability of a polymer with an effective Lennard-Jones interaction parameter $\tilde{u}_{LJ} = \tilde{u}_{EFF}$ that does not interact through binding associations to the interacting probability of a polymer that binds both through associations and through a Lennard-Jones interaction $\tilde{u}_0$. For the latter case, we calculate the interacting probability by a weighted sum of the bound and unbound states by the fractions determined in eq 8, with the bound states always interacting and the unbound states interacting with a probability of $(1 + e^{-z\tilde{u}_0})^{-1}$. This time-averaging results in the following equation:

$$\begin{aligned}(1 + e^{-z\tilde{u}_{EFF}})^{-1} &= f_B + f_{UB}(1 + e^{-z\tilde{u}_0})^{-1} \\ &= 1 - (1 + e^{-\Delta E_0})^{-z} \\ &\quad + [(1 + e^{-\Delta E_0})^z (1 + e^{-z\tilde{u}_0})]^{-1} \end{aligned} \quad (9)$$

The value of z is calculated from simulations to be $\approx 3-4$, and ΔE_0 and $\tilde{u}_0$ are known parameters so it is possible to calculate $\tilde{u}_{EFF}$. The results of this transformation are shown in Figure 5 for polymers of $N = 50$, 100, and 200. Figure 5 shows there to be good correspondence between the reaction-association and Lennard-Jones cases. We point out that no adjustable fit parameters are used in this model and that the parameters of this model are rather sensitive to changes. Adjustments to values of z, ΔE_0, and $\tilde{u}_0$ away from simulation values result in marked changes to the results in Figure 5, suggesting that such a satisfactory correspondence is not simply fortuitous. The success of this model can be attributed to the convenient structure within the globule based on $\langle g_B(n) \rangle$, which demonstrates that the internal structure of the associating globules resembles a homogeneous melt. There is a limitation, though, at high values of $\tilde{u}_{EFF}$. In this regime, the level of collapse of the self-associating globule is consistently less than predicted by a Lennard-Jones model. This can be explained qualitatively by two effects: binding exclusivity, which ensures that the presence of a given binding pair lowers the number of binding options of nearby unbound monomers, and differences in the range of interactions. The latter effect is the result of having a reaction cutoff $\tilde{r}_{rxn} = 2.1$ that is smaller than the interaction length of a Lennard-Jones potential. When the number of neighbors z to a binding monomer becomes large, then this effect becomes significant due to packing limitations which prevent monomers that would otherwise interact

through the Lennard-Jones potential from being close enough to be within $\tilde{r}_{rxn}$.

We emphasize that there is limitation in this type of approach to systems that have a relatively dense distribution of binders along the chain. A number of papers focus specifically on chains with very dilute binder systems (as few as two binders per chain).[18,42,5] Many observe qualitatively similar behavior, such as Baljon, who reports smaller chain structures upon the addition of pairs of "sticking" units that are highly attracted to each other along the chain.[42] These types of situations require different types of theories that take into account looping probabilities that depend on the length of the chain linking two binders.[42] Such chains avoid truly collapsed states, undergo coil−loop transitions, and thus represent a separate class of self-associating polymers. As long as this "dense" binder distribution requirement is met, however, there is now a clear quantitative connection between the binder equilibrium thermodynamics and the Lennard-Jones-type interacting systems that are frequently used in the literature.[36,41,45,47]

This theory can be manipulated to account for other effects, such as the consideration of polymers of other periodicities. To account for this, it is necessary to rewrite eq 9 to include the parameter p, where p is the aforementioned periodicity of the binders:

$$(1 + e^{-z\tilde{u}_{eff}})^{-1} = \left(1 - \frac{1}{p}\right)(1 + e^{-z\tilde{u}_0})^{-1} + \frac{1}{p}[1 - (1 + e^{-\Delta E_0})^{-z/p} + [(1 + e^{-\Delta E_0})^{z/p}(1 + e^{-z\tilde{u}_0})]^{-1}] \quad (10)$$

which accounts for two deviations from the original theory: (1) there are now z/p possible binders surrounding a given binder bead, and (2) only $1/p$ of all beads in the overall chain are binders. This straightforward substitution neglects possible spatial correlations, especially those demonstrated earlier where binding beads tend to partition toward the center of the globule; however, as long as these effects are small, this transformation is still a good approximation. All of the results shown in Figure 4 are now shown on a graph of $\langle R_G^2\rangle/N$ vs $\tilde{u}_{eff}$ (Figure 5) using this transformation. There is very good quantitative agreement between Lennard-Jones interactions and the association-based effective interactions for a variety of values of N and p.

The reasonable agreement between collapse via the Lennard-Jones interactions and collapse via reactive associations, along with the appropriate correlation and conformational behavior, reinforces that the two processes are analogous in terms of equilibrium structure. This provides another route to collapsed conformations in solution and indicates that the comparison between certain biopolymers (specifically, vWF and chromatin) to collapsed homopolymers is worthwhile.

We further supplement this theory by considering the case of multifunctional binders. Intuitively, higher functionality leads to stronger collapse. We demonstrate this by plotting the root-mean-square radius of gyration $\langle R_G^2\rangle^{1/2}$ of monofunctional, difunctional, and trifunctional polymers as a function of ΔE_0. The globule conformation is more driven toward collapse as the functionality increases from 1 to 2, with the results more closely resembling the curve for a Lennard-Jones system once replotted as a function of $\tilde{u}_{eff}$. Difunctionality is incorporated through the replacement of the interaction energy ΔE_0 with an "effective" interaction energy:

$$\Delta E_{0,\,eff} = \Delta E_0\left(\frac{2}{1 + e^{\Delta E_0}} + \frac{1}{1 + e^{-\Delta E_0}}\right) \quad (11)$$

which assumes an equilibrium between singly-bonded and double-bonded states for a difunctional binding. Trifunctionality was also investigated; however, there appears to be no difference between this case versus the difunctional case. This indicates that steric interactions strongly inhibit the formation of such aggregates.

Relaxation Dynamics. Structurally, collapsed globules with associating monomers and collapsed globules with Lennard-Jones-type interactions can be considered equivalent by a number of metrics, as shown in the previous section. All of these measures, however, are determined by large time averages and thus do not consider the dynamics of the polymer. Chain dynamics are critical for rheological behavior, where the relaxation time of a polymer governs its response to applied fluid flows. From a biological perspective, the dynamics of the chain may play critical role in how a biological polymer (such as a protein) interacts with its surroundings, particularly in the presence of external forces. There are also analogues developed in the literature between coil−globule transition kinetics and simple protein folding, and a great deal of effort has gone into characterizing these dynamics in a number of different situations.[39,40,45−49] Theory and simulation have elucidated, for example, some typical conformational pathways that are characteristic of these systems; chains collapsing from extended conformations first develop bead−string morphologies that proceed to sausage-shaped structures that relax into traditional spherical globules.[39,40,45−49] Again, these simulation investigations largely rely on Brownian or molecular dynamics simulations that usually incorporate very standard Lennard-Jones type interactions,[40,44,47,48,54,55] and most recent efforts have focused on refining original bead−spring models by including either hydrodynamic interactions[39,48] or investigate explicit solvent simulations with increasing molecular detail.[41,45,49,54−56] A small number of simulations have used purely Monte Carlo approaches; however, the dynamic information from these simulations is limited.[42,53,57] In contrast to these approaches, which have yielded some interesting results in terms of hydrodynamic cooperativity and solvation effects, we retain a coarse-grained approach and instead examine the effect of Bell-model type associations on chain dynamics.[58] We also depart from much of the previous work in the field by focusing more on the fluctuations around equilibrium collapsed chain structures rather than the far-from-equilibrium collapse transition scenarios which we consider difficult to characterize.

To probe the relaxation dynamics of a single reacting chain, the same BD protocol used for the equilibrium studies is used, only with $>1 \times 10^{10}$ time steps to ensure good averaging. We desire an understanding of both the local and global dynamics, so two different correlation functions are used. To probe local dynamics, we consider a time correlation function that measures the motion of neighboring monomers, $F(\tilde{t})$.[44] This function is constructed from a neighbor matrix $\mathbf{M}_{ij}$ that is defined as

$$\mathbf{M}_{ij} = \begin{cases} 1 & r_{ij} < 3a \text{ and } i \neq (j, j+1, j-1) \\ 0 & \text{otherwise} \end{cases} \quad (12)$$

$F(\tilde{t})$ is then given by

$$F(\tilde{t}) = \frac{1}{N}\sum_i^N \sum_j^N \mathbf{M}_{ij}(\tilde{t}_0)\mathbf{M}_{ij}(\tilde{t}_0 + \tilde{t}) \quad (13)$$

This correlation effectively "tags" and counts the beads that are adjacent to a given monomer that are not directly connected

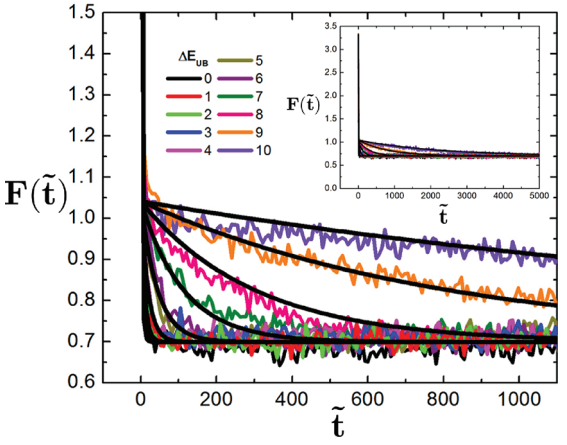

Figure 7. Local correlation factor $F(\tilde{t})$ as a function of $\tilde{t}$ for a variety of values of ΔE_{UB} and fit to eq 15 (black lines) using the values $F(0) = 3.33$, $\phi = 0.21$, and $f_{UB} = 0.87$. $N = 50$, $\Delta E_0 = 0$, and $p = 1$. The main plot shows an enlarged portion of the overall correlation behavior. This clearly shows the important features of this plot, namely the quantitative fit between simulation and 15 for a variety of values of ΔE_{UB}. The inset shows the overall correlation behavior, which demonstrates a very rapid decay at $\tilde{t} \sim 0$ due to the diffusion of unbound beads.

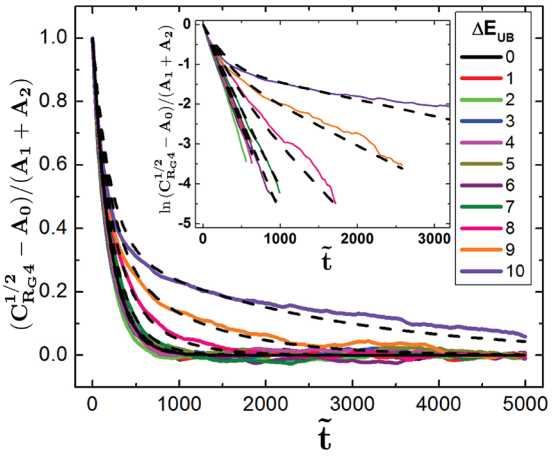

Figure 8. Normalized global correlation factor $(C_{R_G^4}{}^{1/2} - A_0)/(A_1 + A_2)$ as a function of $\tilde{t}$ for a variety of values of ΔE_{UB} and fit to eq 19 (dashed lines) using the values $\tau_R = 195$ and $A_2/(A_1 + A_2) = 0.35$. $N = 50$, $\Delta E_0 = 0$, and $p = 1$. In the inset, the same data are plotted on a semilog plot of $\ln((C_{R_G^4}{}^{1/2} - A_0)/(A_1 + A_2))$ vs $\tilde{t}$. This clearly shows the emergence of the second time scale at large ΔE_{UB}, in agreement with the double-exponential fit used.

along the chain at time $\tilde{t}_0$. The number of tagged beads that remain nearby at time $\tilde{t}_0 + \tilde{t}$ is given by $F(\tilde{t})$, with $F(\infty)/F(0)$ roughly representing the volume fraction of the coil taken up by the initially tagged beads. In a collapsed polymer, this can be exactly calculated to be $F(\infty)/F(0) = F(0)[4\pi a^3/(3V_{av})]$, where $V_{av} = 4N\pi a^3/(3f)$ is the available volume in which initially tagged beads can explore (f is a geometric packing factor representing bead density). This measure provides a local description of the dynamics, where we expect to see both the decay behavior attributed to regular monomer diffusion (Rouse dynamics) and the decay behavior attributed to binder disassociation. Given these two behaviors, we can postulate a double-exponential form of $F(\tilde{t})$:

$$F(\tilde{t}) = F(\infty) + F_{UB}e^{-t/\tau_1} + F_B e^{-t/\tau_{Bind}} \quad (14)$$

where F_{UB} and F_B are related to the average number of unbound and bound tagged molecules, respectively. The contribution of the various prefactors is given by the fraction of bound monomers at a given time f_B, such that the equation can be expressed as a function of chain parameters such as $F(0)$, $\tau_1 \sim 1$, $\tau_{Bind} \sim 1 + \tau_0 e^{\Delta EU_B}$, and f_B:

$$F(\tilde{t}) = F(0)[\phi + (1 - f_B)(1 - \phi)e^{-\tilde{t}} + f_B(1 - \phi)e^{-\tilde{t}/\tau_{Bind}}] \quad (15)$$

where $\phi = F(0)f/N$ is the volume fraction of initially tagged beads. The value of $\tau_1 \sim 1$ is chosen since it represents the diffusive time of a single monomer, which is appropriate for an unbound bead, and $\tau_{Bind} \sim 1 + \tau_0 e^{\Delta EU_B}$ represents the serial two-step process of unbinding and then diffusion that is the relaxation process for a bound bead, with the latter step requiring the former in order to proceed. This theory demonstrates excellent agreement with the simulation data, and both simulation and theory are plotted in Figure 7 for $N = 50$, $\Delta E_0 = 0$, and $p = 1$. Importantly, the binding and unbinding attempts in these simulations occur much more frequently than this local relaxation time and thus account for rebinding effects like those seen in the literature.[21−23]

The local binder/diffusion relaxation behavior at monomer length scales manifests itself in dynamic changes at chain length scales. We calculate the following correlation function $C_{R_G^4}$:

$$\begin{aligned} C_{R_G4}(t) &= \langle R_G{}^2(0) R_G{}^2(t) \rangle \\ &= \{\int_0^\infty [\sum_i^N (\mathbf{r}_i(t') - \mathbf{r}_{com}(t'))^2][\sum_i^N (\mathbf{r}_i(t' + t) \\ &\quad - \mathbf{r}_{com}(t' + t))^2]\, dt'\}/\{N^2 \int_0^\infty dt'\} \end{aligned} \quad (16)$$

This correlation function is advantageous due to its reliance on the entire chain conformation, rather than more traditional correlation functions such as those related to the end-to-end distance. This means that the correlation function $C_{R_G^4}$ is more sensitive to the existence of any long-lasting structural features. For a nonassociating Θ-polymer, it is related to the relaxation time through the relationship

$$C_{R_G4} = \langle R_G{}^2(0) \rangle^2 + (\langle [R_G{}^2(0)]^2 \rangle - \langle R_G{}^2(0) \rangle^2) e^{-t/\tau_R} \quad (17)$$

where $\langle [R_G{}^2(0)]^2 \rangle$ is the instantaneous value of the mean-square radius of gyration squared. This equation can be derived using Rouse theory.[2] Likewise

$$C_{R_G4}{}^{1/2} \approx \langle R_G{}^2(0) \rangle \left(1 + \frac{\alpha}{2} e^{-t/\tau_R}\right) \quad (18)$$

where $\alpha = (\langle [R_G{}^2(0)]^2 \rangle - \langle R_G{}^2(0) \rangle^2)/(\langle R_G{}^2(0) \rangle^2)$. For Θ-polymers, $\alpha_\Theta = 4/15$.[59] We plot $C_{R_G^4}{}^{1/2}$ normalized so that it goes from 1 to 0 for a number of conditions in Figure 8. Plots of these functions are often well fit by the single-exponential function that this formula suggests if relaxation occurs rapidly. For longer time scale self-associations, however, another time scale is needed and a double exponential function is used:

$$C_{R_G4}{}^{1/2} = A_0 + A_1 e^{-t/\tau_1} + A_2 e^{-t/\tau_2} \quad (19)$$

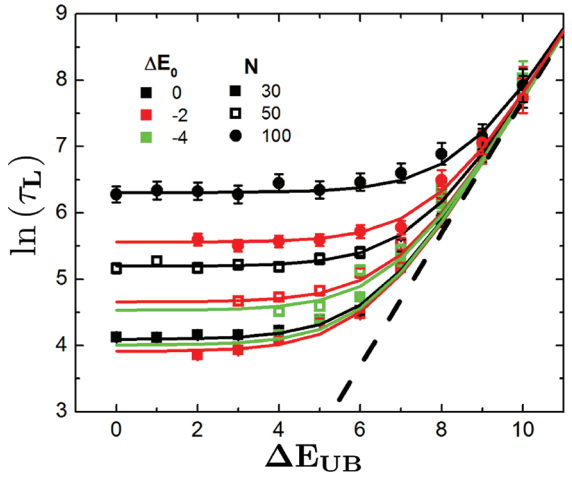

Figure 9. $\ln \tau_L$ as a function of the unbinding energy ΔE_{UB} for a $N = 30$ (filled squares), $N = 50$ (open squares), and $N = 100$ (circles) with $\Delta E_0 = 0$ (black symbols), $\Delta E_0 = -2$ (red symbols), and $\Delta E_0 = -4$ (green symbols). Both simulation data (symbols) and theory (lines) are shown, with the Rouse time τ_R chosen to match the simulation data. Two regimes are apparent—at low ΔE_{UB} relaxation is dominated by Rouse motion, while at high ΔE_{UB} relaxation is dominated by binder kinetics. The theoretical time scale of a single binder is shown by the dotted, thick black line which matches up well with the binder kinetic regime for all curves at large ΔE_{UB}.

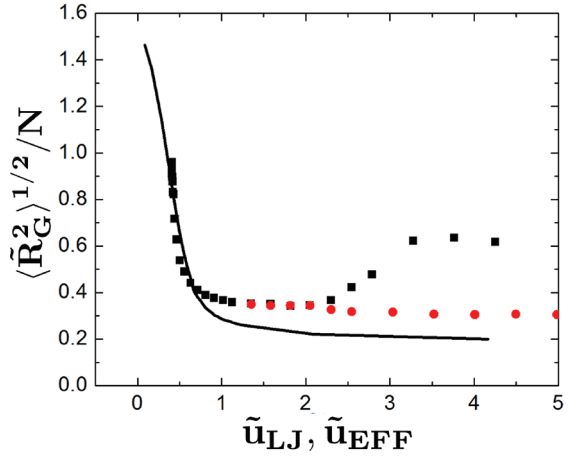

Figure 10. $\langle R_G^2 \rangle^{1/2}$ vs $\tilde{u}_{eff}$ for $N = 50$. As the value of ΔE_{UB} ($\Delta E_B = 0$) is increased and the globule is collapsed, the initial state of the globule has an effect on its size at the time scale of the simulation (5×10^8 time steps). If the initial configuration is elongated (black points), there is a finite time for the collapsed structure to become realized. If the structure does not have the ability to relax fully in the time scale of the simulation, it remains larger than equilibrium collapsed conformation. This is seen in the points above $\tilde{u}_{eff} > 2$, where ΔE_{UB} is large. If the globule is collapsed by slowly increasing the value of ΔE_{UB} (red points), the resulting size is closer to the equilibrium collapsed structure. The solid black line indicates the collapse of a Lennard-Jones system with respect to the interaction parameter $\tilde{u}_{LJ}$. Error bars are smaller than the size of the data points.

where A_0, A_1, and A_2 are fit constants that are related to the equilibrium polymer structure ($A_0 = \langle R_G^2(0) \rangle^2$, $A_0 + A_1 + A_2 = \langle [R_G^2(0)]^2 \rangle$) and the relative contribution to $\langle R_G^2 \rangle$ of the portion of the chain that is initially constrained due to self-associations (A_2). For the data represented in Figure 8, the proportion of the $\langle R_G^2 \rangle$ value that contains contributions from the constrained section of the chain is about 35%, which is reasonably larger than the fraction ($f_B \approx 13\%$) of bound monomers for the same conditions. This is expected due to the binders constraining both the bound monomers and their neighbors as well. The appearance of a second relaxation time scale is clearly shown in the inset of Figure 8, which replots the decay functions in a semilog plot. While low values of ΔE_{UB} demonstrate straight line behavior expected of a single exponential, this transitions into a kinked-line geometry characteristic of a double-exponential decay like the one proposed in eq 19. This equation fits all curves and suggests the existence of at least two time scales present in the relaxation of the polymer. To reinforce the binder/diffusion mechanism at monomer length scales, we postulate an analogous binder/Rouse global relaxation mechanism. These time scales thus correspond to the Rouse relaxation time $\tau_1 = \tau_R$ and the binder relaxation time plus the Rouse relaxation time $\tau_2 = \tau_L = \tau_R + \tau_B = \tau_R + \tau_0 e^{\Delta E_0}$. We consider the latter the "effective" longest-time scale $\tau_L = \tau_R + \tau_0 e^{\Delta E_0}$ as the critical description of the chain structural relaxation. This description of τ_L again considers that the two kinetic processes of unbinding and then diffusive chain relaxation are serial in time and thus their time scales are additive. This theoretical description of the size correlation function $C_{R_G^4}^{1/2}$ is demonstrated alongside the simulation data for $N = 50$ in Figure 8, also normalized so that the function goes from $C_{R_G^4}^{1/2} = 1$ to 0. There is a good fit between the two sets of data.

We plot the natural log of the longest relaxation time τ_L as a function of the unbinding energy ΔE_{UB} for a number of values of N and ΔE_0 in Figure 9. It is important to note that each curve represents a single equilibrium structure that is independent of the value of ΔE_{UB}. This value does alter the dynamics significantly, however, with all curves collapsing at large ΔE_{UB} on an exponential dependence of ΔE_{UB} that appears to be universal. This is plotted alongside the binder relaxation time $\tau_B = \tau_0 e^{\Delta E_0}$ (dotted line), which fits this regime very well. This suggests that there is a transition into a regime where the time scale is governed by individual binders that "pin" structural characteristics for as long as that association is present. At low values of ΔE_{UB}, the dynamics are governed by the normal relaxation of a nonhydrodynamic interacting chain. Indeed, it would be trivial to translate these results to the case of a chain model that incorporates hydrodynamic interactions by replacing the Rouse time τ_R with the Zimm relaxation time τ_Z.

The dependence of a polymer's dynamics on its binding kinetics is clearly observed qualitatively given the relaxation of these polymers from an extended state. This type of relaxation process is well documented in the literature, despite its far-from-equilibrium nature, due to its relevance to protein folding kinetics.[39,40,45−49] We do not perform an in-depth study of this process but qualitatively demonstrate that the dynamics are indeed strongly altered even in a nonequilibrium case. Movies in the Supporting Information show this relaxation in polymers that have the same ΔE_0 but very different values of ΔE_{UB}. While there is quick relaxation for a polymer with $\Delta E_{UB} = 4.0$ well within the time scale of the movie, the polymer with $\Delta E_{UB} = 10.0$ never seems to completely relax. This behavior manifests itself in a bifurcation seen in Figure 10 for large values of ΔE_{UB}, where the plot of $\langle R_G^2 \rangle / N$ vs $\tilde{u}_{eff}$ continues the predicted trend only if the polymer starts in a precollapsed state (gray symbols) but has much larger chain dimensions than predicted if relaxed from an

extended state (black symbols). In principle, the polymer starting from the extended state would end up relaxing to the collapsed state in the limit of infinite time; however, for our finite-time simulations this process can be limited by slow reaction kinetics. This bifurcated system therefore represents the only system presented in this investigation where the length of the run is no longer larger than the relaxation time of the system, accomplished by simply changing the nature of the binding kinetics. Such behavior could have ramifications in the response of association-collapsed chains in flows and could lead to interesting rheological memory effects.

CONCLUSIONS

In this paper we have shown that, in analogy to simpler Lennard-Jones models, the presence of associating groups along a polymer chain can induce chain collapse into a globule polymer structure. We have developed Brownian dynamics simulations that couple to Bell model-inspired reaction kinetics to emulate the behavior of a self-associating polymer. These types of associations are ubiquitous in polymeric materials, with this type of model representing features such as hydrogen bonding, metalloorganic complexation, and reversible covalent bonds. This type of interaction has already been very important in the design of novel responsive materials, and here we consider the single-chain analogue. Through these simulations, it has been demonstrated that these collapsed polymers demonstrate the same structural characteristics as those obtained through Lennard-Jones interactions, and by using a mean-field model, it is possible to provide a direct correspondence between the parameters of a Lennard-Jones model and a reaction-based model. This correspondence is capable of being modified to incorporate a number of effects, including multifunctionality and periodic binding; however, we expect there to be limits to the latter due to the tendency of associating units that are separated by long nonassociating chains to form "flower micelle" conformations. This property, however, may be useful in the creation of solutions of collapsed polymers that are resistant to macroscopic phase separation.

From a dynamical standpoint, by incorporating associating groups with large energy barriers, we show that it is possible to increase and controllably manipulate the relaxation time scale of a single polymer chain without changing the equilibrium chain conformation. This is due to the longevity of "clusters" of monomers around two associating monomers, resulting in long time-scale correlations. The addition of a relaxation time scale that is governed by association kinetics rather than chain characteristics has implications on most dynamic properties of a single chain. For example, this would drastically change the rheological behavior of a solution of these molecules, whose deformation behavior of flow is intimately tied to the reorganization time scale of a polymer chain. The abundance of these types of interactions in biological polymers, which work in concert with interactions that have more rapid dynamics (hydrophobic and dispersive forces, for example), suggests that these results are also important in the behavior of biological materials.

ASSOCIATED CONTENT

Supporting Information. Movies that demonstrate the dynamic relaxation behavior of two self-associating polymers with the same ΔE_0 but different values of ΔE_{UB}. In movie 1, $\Delta E_{UB} = 4.0$, which yields rapid relaxation behavior. In movie 2, $\Delta E_{UB} = 10.0$, which never seems to fully relax over the course of the movie. For both movies, $\Delta E_0 = -3.0$, $N = 100$, and they occur over 10000τ. Orange links represent the contour of the polymer, while purple links represent binding associations. This material is available free of charge via the Internet at http://pubs.acs.org.

AUTHOR INFORMATION

Corresponding Author
*E-mail: aalexand@mit.edu.

ACKNOWLEDGMENT

We acknowledge financial support from the National Defense Science and Engineering Graduate Fellowship, NSF CAREER Award #1054671, and computational support from Teragrid allocation TG-DMR090139.

REFERENCES

(1) de Gennes, P. G. *Scaling Concepts in Polymer Physics*; Cornell University Press: Ithaca, NY, 1979.
(2) Doi, M.; Edwards, S. *The Theory of Polymer Dynamics*; Oxford University Press: Ithaca, NY, 1986.
(3) Petka, W.; Harden, J.; McGrath, K.; Wirtz, D.; Tirrell, D. *Science* **1998**, *281*, 389–392.
(4) Kushner, A. M.; Vossler, J. D.; Williams, G. A.; Guan, Z. *J. Am. Chem. Soc.* **2009**, *131*, 8766.
(5) Ilmain, F.; Tanaka, T.; Kokufuta, E. *Nature* **1991**, *349*, 400–401.
(6) Wojtecki, R. J.; Meador, M. A.; Rowan, S. J. *Nature Mater.* **2011**, *10*, 14–27.
(7) Weng, W.; Jamieson, A. M.; Rowan, S. J. *Tetrahedron* **2007**, *63*, 7419–7431.
(8) Kushner, A. M.; Gabuchian, V.; Johnson, E. G.; Guan, Z. *J. Am. Chem. Soc.* **2007**, *129*, 14110–+.
(9) Annable, T.; Buscall, R.; Ettelaie, R.; Whittlestone, D. *J. Rheol.* **1993**, *37*, 695–726.
(10) Erk, K. A.; Shull, K. R. *Macromolecules* **2011**, *44*, 932–939.
(11) Leibler, L.; Rubinstein, M.; Colby, R. H. *Macromolecules* **1991**, *24*, 4701–4707.
(12) Semenov, A. N.; Joanny, J. F.; Khokhlov, A. R. *Macromolecules* **1995**, *28*, 1066–1075.
(13) Semenov, A.; Rubinstein, M. *Macromolecules* **2002**, *35*, 4821–4837.
(14) Cifre, J.; Barenbrug, T.; Schieber, J.; van den Brule, B. *J. Non-Newtonian Fluid Mech.* **2003**, *113*, 73–96.
(15) Ayyagari, C.; Bedrov, D.; Smith, G. D. *Polymer* **2004**, *45*, 4549–4558.
(16) Tripathi, A.; Tam, K. C.; McKinley, G. H. *Macromolecules* **2006**, *39*, 1981–1999.
(17) Han, X.-G.; Zhang, C.-X. *J. Chem. Phys.* **2010**, *132*, 164905.
(18) Li, Z.; Djohari, H.; Dormidontova, E. E. *J. Chem. Phys.* **2010**, *133*, 184904.
(19) Wang, S.; Chen, C.-C.; Dormidontova, E. E. *Soft Matter* **2008**, *4*, 2039–2053.
(20) Hoy, R. S.; Fredrickson, G. H. *J. Chem. Phys.* **2009**, *131*, 224902.
(21) Rubinstein, M.; Semenov, A. N. *Macromolecules* **1998**, *31*, 1386–1397.
(22) Rubinstein, M.; Semenov, A. N. *Macromolecules* **2001**, *34*, 1058–1068.
(23) Semenov, A. N.; Rubinstein, M. *Macromolecules* **1998**, *31*, 1373–1385.
(24) Evans, E.; Ritchie, K. *Biophys. J.* **1997**, *72*, 1541–1555.
(25) Kenward, M.; Dorfman, K. D. *J. Chem. Phys.* **2009**, *130*, 095101.
(26) Sheng, Y. J.; Lin, H. J.; Chen, J. Z. Y.; Tsao, H. K. *Macromolecules* **2004**, *37*, 9631–9638.

(27) Thomas, W. E.; Vogel, V.; Sokurenko, E. *Annu. Rev. Biophys.* **2008**, *37*, 399–416.
(28) Pande, V. S.; Grosberg, A. Y.; Tanaka, T.; Rokhsar, D. S. *Curr. Opin. Struct. Biol.* **1998**, *8*, 68–79.
(29) Capadona, J. R.; Shanmuganathan, K.; Tyler, D. J.; Rowan, S. J.; Weder, C. *Science* **2008**, *319*, 1370–1374.
(30) Nichifor, M.; Lopes, S.; Bastos, M.; Lopes, A. *J. Phys. Chem. B* **2004**, *108*, 16463–16472.
(31) Pande, V. S.; Grosberg, A. Y.; Tanaka, T. *Rev. Mod. Phys.* **2000**, *72*, 259–314.
(32) Greenleaf, W. J.; Woodside, M. T.; Block, S. M. *Annu. Rev. Biophys. Biomol. Struct.* **2007**, *36*, 171–190.
(33) Alexander-Katz, A.; Wada, H.; Netz, R. R. *Phys. Rev. Lett.* **2009**, *103*, 028102.
(34) Mateos-Langerak, J.; Bohn, M.; de Leeuw, W.; Giromus, O.; Manders, E. M. M.; Verschure, P. J.; Indemans, M. H. G.; Gierman, H. J.; Heermann, D. W.; Driel, R. V.; Goetze, S. *Proc. Natl. Acad. Sci. U.S.A.* **2009**, *106*, 3812–3817.
(35) Bohn, M.; Heermann, D. W. *PLoS One* **2010**, *5*, e12218.
(36) Alexander-Katz, A.; Netz, R. R. *Macromolecules* **2008**, *41*, 3363–3374.
(37) Grosberg, A. Y.; Kuznetsov, D. V. *Macromolecules* **1992**, *25*, 1970–1979.
(38) Williams, C.; Brochard, F.; Frisch, H. L. *Annu. Rev. Phys. Chem.* **1981**, *32*, 433–451.
(39) Kikuchi, N.; Ryder, J. F.; Pooley, C. M.; Yeomans, J. M. *Phys. Rev. E* **2005**, *71*, 061804.
(40) Pham, T. T.; Duenweg, B.; Prakash, J. R. *Macromolecules* **2010**, *43*, 10084–10095.
(41) Polson, J. M.; Zuckermann, M. J. *J. Chem. Phys.* **2002**, *116*, 7244–7254.
(42) Baljon, A. R. C. *Macromolecules* **1993**, *26*, 4339–4345.
(43) Kantor, Y.; Kardar, M. *Europhys. Lett.* **1994**, *28*, 169–174.
(44) Sing, C. E.; Einert, T. R.; Netz, R. R.; Alexander-Katz, A. *Phys. Rev. E* **2011**, *83*, 040801.
(45) Chang, R. W.; Yethiraj, A. *J. Chem. Phys.* **2001**, *114*, 7688–7699.
(46) Xie, R.; Weiss, R. *Comput. Theor. Polym. Sci.* **1997**, *7*, 65–74.
(47) Polson, J. M.; Moore, N. E. *J. Chem. Phys.* **2005**, *122*, 024905.
(48) Das, S.; Chakraborty, S. *J. Chem. Phys.* **2010**, *133*, 174904.
(49) Tanaka, G.; Mattice, W. L. *Macromolecules* **1995**, *28*, 1049–1059.
(50) Sing, C. E.; Alexander-Katz, A. *Macromolecules* **2010**, *43*, 3532–3541.
(51) Grosberg, A. Y.; Khokhlov, A. R. *Statistical Physics of Macromolecules*; American Institute of Physics: Melville, NY, 1994.
(52) Lifshitz, I. M.; Grosberg, A. Y.; Khokhlov, A. R. *Rev. Mod. Phys.* **1978**, *50*, 683–713.
(53) Tsao, H. K.; Chen, J. Z. Y.; Sheng, Y. J. *Macromolecules* **2003**, *36*, 5863–5872.
(54) Zhou, R. H.; Huang, X. H.; Margulis, C. J.; Berne, B. J. *Science* **2004**, *305*, 1605–1609.
(55) Athawale, M. V.; Goel, G.; Ghosh, T.; Truskett, T. M.; Garde, S. *Proc. Natl. Acad. Sci. U.S.A.* **2007**, *104*, 733–738.
(56) Goel, G.; Athawale, M. V.; Garde, S.; Truskett, T. M. *J. Phys. Chem. B* **2008**, *112*, 13193–13196.
(57) Ivanov, V.; Stukan, M.; Vasilevskaya, V.; Paul, W.; Binder, K. *Macromol. Theory Simul.* **2000**, *9*, 488–499.
(58) Bell, G. I. *Science* **1978**, *200*, 618–627.
(59) Rubinstein, M.; Colby, R. *Polymer Physics*; Oxford University Press: Ithaca, NY, 2003.